J. Electrochem. Sci. Eng. **12(3)** (2022) 501-510; http://dx.doi.org/10.5599/jese.1280

Open Access : : ISSN 1847-9286

https://pub.iapchem.org/ojs/index.php/JESE

Original scientific paper

Root cause analysis of the corrosion-related coiled tubing failure

Sanja Martinez[1], Fuad Khoshnaw[2], Vuokko Heino[3], Sara Fahmi[4], Talal A. Aljohani[5,✉] and Sally Elkatatny[6]

[1]*Research Laboratory for Corrosion Engineering and Surface Protection - ReCorr, Department of Electrochemistry, Faculty of Chemical Engineering and Technology, University of Zagreb, Croatia*
[2]*School of Engineering and Sustainable Development, Faculty of Computing, Engineering and Media, De Montfort University, Leicester, United Kingdom*
[3]*VTT Technical Research Centre of Finland Ltd, P.O. Box 1000, 02044, VTT, Finland*
[4]*Materials Management Consultant, Infosys Ltd., 6002 Rogerdale Road, Houston, USA*
[5]*Materials Science Research Institute, King Abdulaziz City for Science and Technology (KACST), Riyadh, 12354, Saudi Arabia*
[6]*Mechanical Engineering Department, Faculty of Engineering, Suez Canal University, Ismailia, 41522, Egypt*

Corresponding author: ✉taljohani@kacst.edu.sa

Received: February 3, 2022; Accepted: March 1, 2022; Published: March 13, 2022

Abstract

Coiled tubing (CT) is widely used in the oil and gas industry. However, corrosion-related failures are frequently reported. Research into the causes of failures leads to improvement in the design of components and processes. In this study, a new CT sample and a CT sample with perforated wall that had failed after a few acidizing operations were selected for analysis. Scanning electron microscope (SEM) images at the fracture site showed that CT damage was caused by the low cycle fatigue. In addition, light and scanning electron microscopy (SEM) showed that a corrosion pit acted as the initiator of the crack. Elemental analysis using energy dispersive X-ray spectroscopy (EDS) indicated the presence of an iron oxide layer and a layer associated with the Sb containing inhibitor. The corrosion damage investigation showed that the internal CT wall pits likely formed during storage due to the acidizing operations in the areas where the remaining liquid was still at the tube bottom.

Keywords

Coil tubing; corrosion; failure analysis; microbiological induced corrosion

Introduction

Coiled tubing technology (CT) is widely used in well operations [1,2]. CT application can be divided into two general categories, fluid pumping and mechanical applications. CT is frequently affected by failures due to various causes [3,4]. Therefore, knowledge of different nomenclatures is required to

diagnose the causes of failure. The causes considered to be the main reasons for the failure of CT can be classified as follows [4-6]:

- Mechanical damage: premature failure of the CT string caused by mechanical means such as fatigue, buckling, yielding, *etc*.
- Corrosion: premature failure of the CT string caused by corrosive environments during well servicing and workovers.
- Manufacturing defect: defects are generated during the original manufacturing process of the coiled tubing, such as material defect, temper embrittlement or cold weld.
- Human error: faults or mistakes during coiled tubing string operations.
- Microbiological induced corrosion (MIC): involves microbes or bacteria within contact with the coiled tubing.
- External abrasion: a localized reduction in wall thickness, generally caused by friction between the coiled tubing and the wall of the well.
- Hydrogen cracking due to H_2S: cracks after the material is exposed to H_2S in the well.

CT corrosion occurs in contact with the atmosphere, pumped and production fluids. Corrosion can significantly shorten tubing life and must be prevented. In particular, localized corrosion can be a trigger for fatigue cracking growth during cycling. In addition, corrosion can affect the strength and pressure resistance of the pipes. Statistical analysis of the CT failure causes was conducted [7] showing that mechanical damage, corrosion, manufacturing flaws, and human error were the main diagnoses for CT failures from 1994 to 2005. These four major causes also represented 80 to 90 % of the failures from 2006 to 2017.

Van Arnam *et al.* [8] reported that corrosion can occur on CT strings from the day of production if they were not properly protected with a corrosion inhibitor. When the temperature of CT reaches the dew point the moisture condenses on the CT surface immediately causing rusting. The rust layer consists of hydrated iron oxides, $Fe(OH)_2$ and $Fe(OH)_3$, or their dry counterparts, hematite (Fe_2O_3) and magnetite (Fe_3O_4). In addition, the presence of chlorides, sulfates or carbon dioxide increases the corrosion rate.

To prevent corrosion, several corrective actions are taken, including revising N_2 purging practices, trail runs with new inhibitors, and seeking feedback from operations to optimize inhibition plans while not increasing operational burden [7,9,10]. Nevertheless, the combination of mechanical and corrosive actions during operations eventually leads to the development of fatigue cracks. It has been found that the growth of fatigue cracks is greater at low-stress cycles, which allows more time for the corrosion process [11].

Unpredictable CT service life is a serious economical and safety issue for the industry. It results from the inadequate in-service inhibition and lacking tubing maintenance programs that do not include storage corrosion prevention. Maximizing CT service life requires effective corrosion control on both sides of the CT wall, during storage and in service.

Experimental

Materials and methods

The current study examined the new and the failed CT samples. The failed CT sample, taken from the wellbore after only few well acidizing jobs with 15 % HCl, contained a perforated wall that was later cut open to expose the fracture area that was also studied. The specified composition of the CT-80 material of the tubes is illustrated in Table 1.

Table 1. *Elemental composition of the coiled tubing material*

Element	C	Mn	P	S	Si	Cu	Ni	Cr	Mo
Content, wt.%	0.06	0.88	0.012	0	0.15	0.2	0.14	0.47	0.14

Bruker Vertex 70 FTIR was used to measure the FTIR spectra of the corrosion products. A scanning electron microscope with energy dispersive spectrometry SEM FEI FEG250QUANTA/ OXFORD EDS PENTAFET was used to study the surface morphology and elemental composition of the fracture. A DURAMIN 2 STRUERS microhardness tester was used to test Vickers microhardness on the base metal and near the fracture surface.

Results and discussion

Visual examination of a new CT sample revealed no corrosion damage to the tubing, as shown in Figure 1. A uniform black coating, visually consistent with the corrosion protection applied by the CT manufacturer, was visible on both sides of the CT wall. In addition, surface rust is visible on the exterior wall of CT (Figure 1a) where the black coating is likely mechanically damaged. No rust was observed on the interior wall of CT (Figure 1b). The black coating was not damaged because the interior wall is protected from mechanical impact.

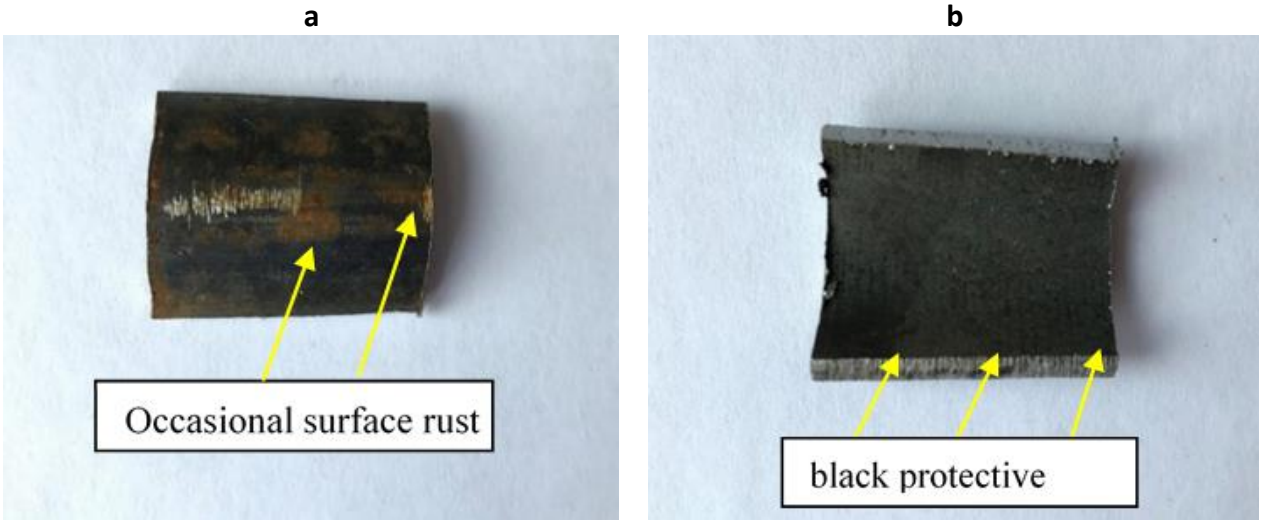

Figure 1. *New coiled tubing: a - outer surface and b - inner surface*

The used CT sample from the well had a metallic appearance on the outside with no visible corrosion products. On the inside, the sample was covered by a layer of brown corrosion products (Figure 2). A black-green corrosion product streak was observed longitudinally across approximately 20 % of the inner diameter.

Figure 3 shows the corrosion pits and Figure 4a shows the cracks, both of which occur only within a black-green area. One of the cracks observed on the inside protruded through the wall of CT and was visible on the outside surface, as shown in Figure 4b.

For close observation and examination, the sample was cut open to expose the fracture surface (Figure 5a). The edge of the corrosion damage in Figure 5b is the source of the striation marks and therefore likely served as the fracture origin. In the central part of the wall, a large area of striation marks perpendicular to the fracture direction was observed. The striations represent the propagation front of the fatigue crack and indicate that the fracture was caused by material fatigue. The Y-shaped crack ends shown in Figure 4b, also support the fatigue hypothesis. In addition, ridges have formed along the inner edge of the fracture parallel to the direction of fracture propagation, which can be

attributed to micro-cracking outside the central fracture plane. Terraces (stepped structures) are formed along the edges of the fracture, which are due to the initial development of the fracture in different planes.

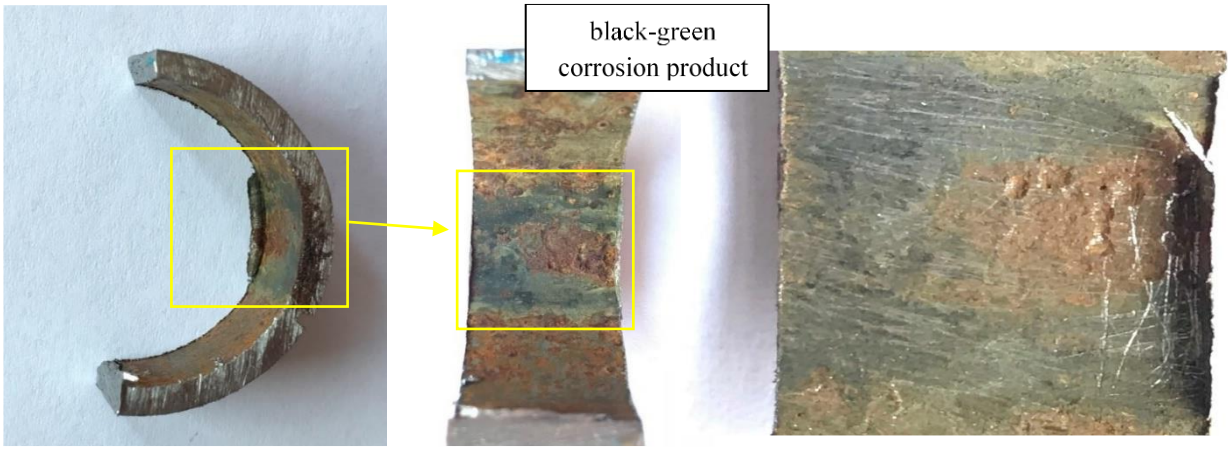

Figure 2. *Black-green corrosion product streak on a coiled tubing sample from the well*

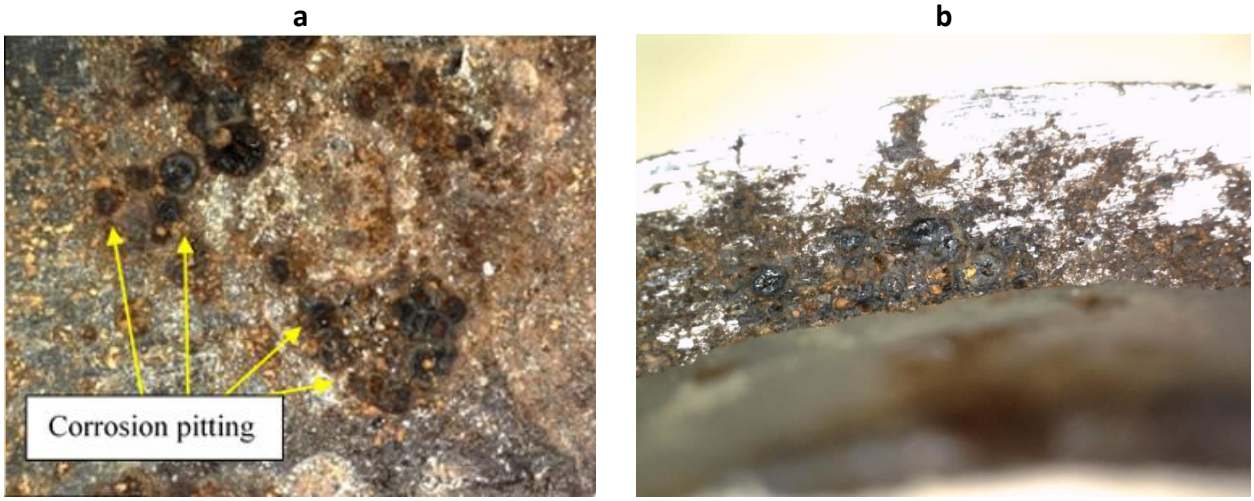

Figure 3. *Corrosion pits on the inner wall of the coiled tubing*

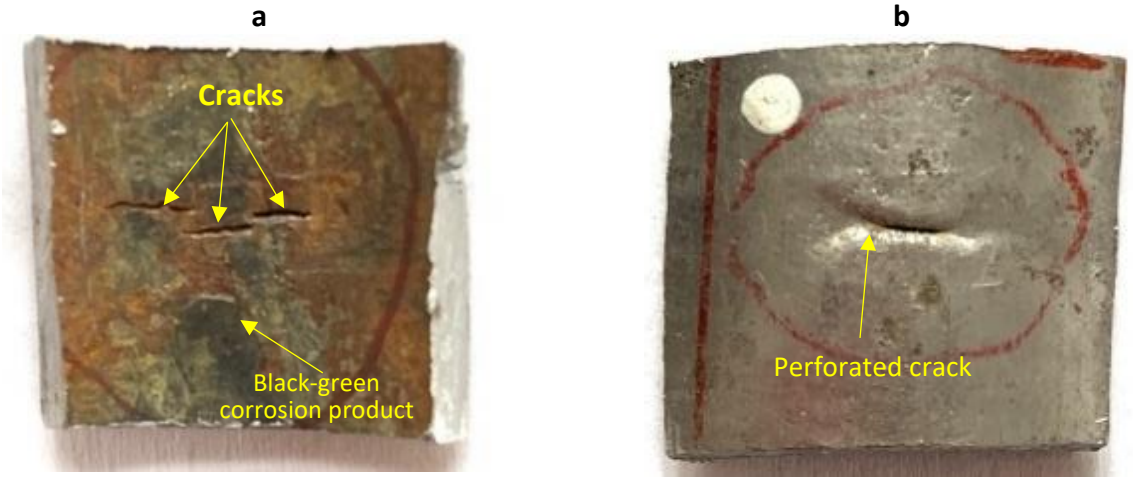

Figure 4*. Cracks on a - the inner surface and b - the outer surface*

The uniformity of striations indicates the homogeneity of the metallurgical structure of the material. The spacing between the striations usually gives information about the growth rate of the cracks (µm/cycle).

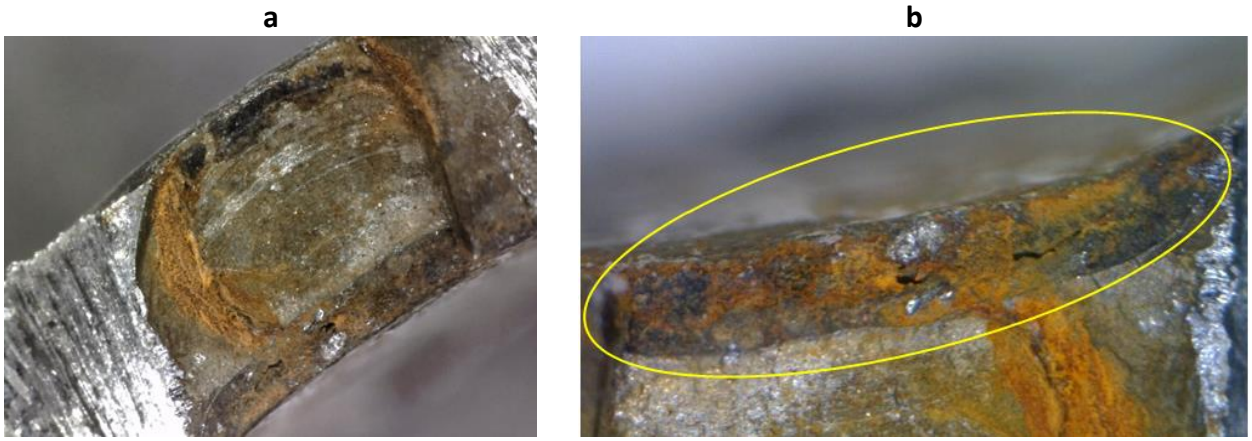

***Figure 5**. Light microscope photographs of a - fracture surface and b - fracture initiation site*

The number of striations is greater than the number of tube straightening and bending cycles, which may indicate a corrosion-related fatigue fracture. As the tip region of the fracture is repeatedly covered with a layer of corrosion products, the growth of the striation mark slows down. It can be argued that the numerous striation marks are due to the acceleration and deceleration of the growth of a fracture during each cycle. Becker and Lampman [12] reported that under many loading conditions, the pre-existing macroscopic crack-like defect blunts with increasing load and a new crack form by ductile tearing, creating a striation zone. Consequently, continued increase in loading causes the crack propagation mechanism to change to cleavage or quasi-cleavage.

The internal surface shown in Figure 3a was examined under a metallographic microscope (Figure 6) and the corrosion pits contained a black corrosion product. Brown-orange corrosion product was seen above the black one on the surface of the shallower defects. The appearance of the corrosion damage suggests atmospheric corrosion of the steel with unobstructed oxygen flow outside the pit and a de-aerated space at the bottom of the pit. The corrosion, more pronounced on the inner diameter, is in good agreement with Still and Rolovic [13].

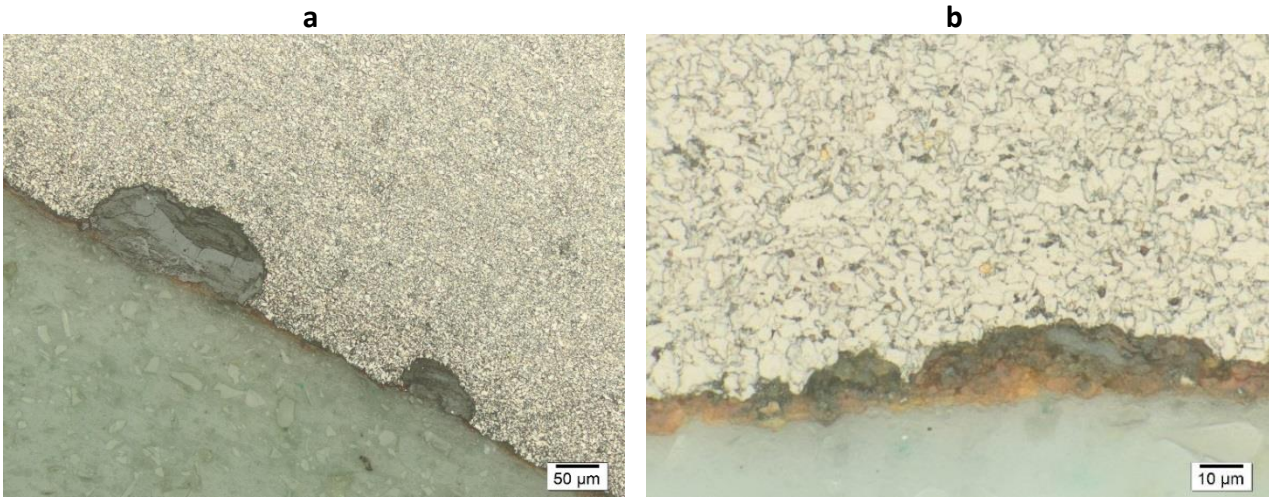

***Figure 6.** The corroded inner surface at different zones*

The polished and etched used CT had a fine-grained microstructure (ASTM sizes 13 to 14) with evenly distributed areas of ferrite and pearlite and some bainite, as shown in Figure 7a. Short banded structures of pearlite are observed in some places in the centre of the wall section (Figure 7b). No cracks are visible on the metallographic samples.

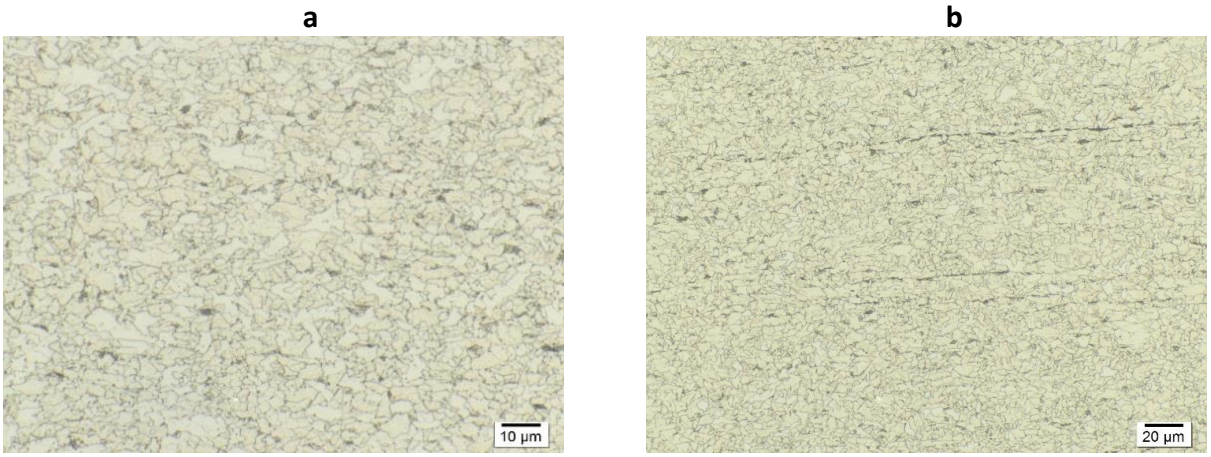

Figure 7. *Fine-grained structure of quasi-polygonal ferrite with uniformly distributed areas of pearlite and bainite*

The layers on the inner surfaces of the new and used CT samples were rubbed with KBr, which was later pressed into pellets for FTIR analysis. The FTIR spectrum of the new CT sample, Figure 8a, shows no clear bands of iron oxides, confirming the absence of corrosion on the inner diameter of the new CT sample. The observed bands indicate the presence of an organic corrosion inhibitor used by the manufacturer of the CT. The FTIR spectrum of the used sample CT is shown in Figure 8b and indicates the presence of antimony oxide. Antimony salts were used as a component of the acidizing corrosion inhibitor and the inner surface of CT is partially covered with deposited metallic antimony, which oxidizes to antimony oxide when exposed to air.

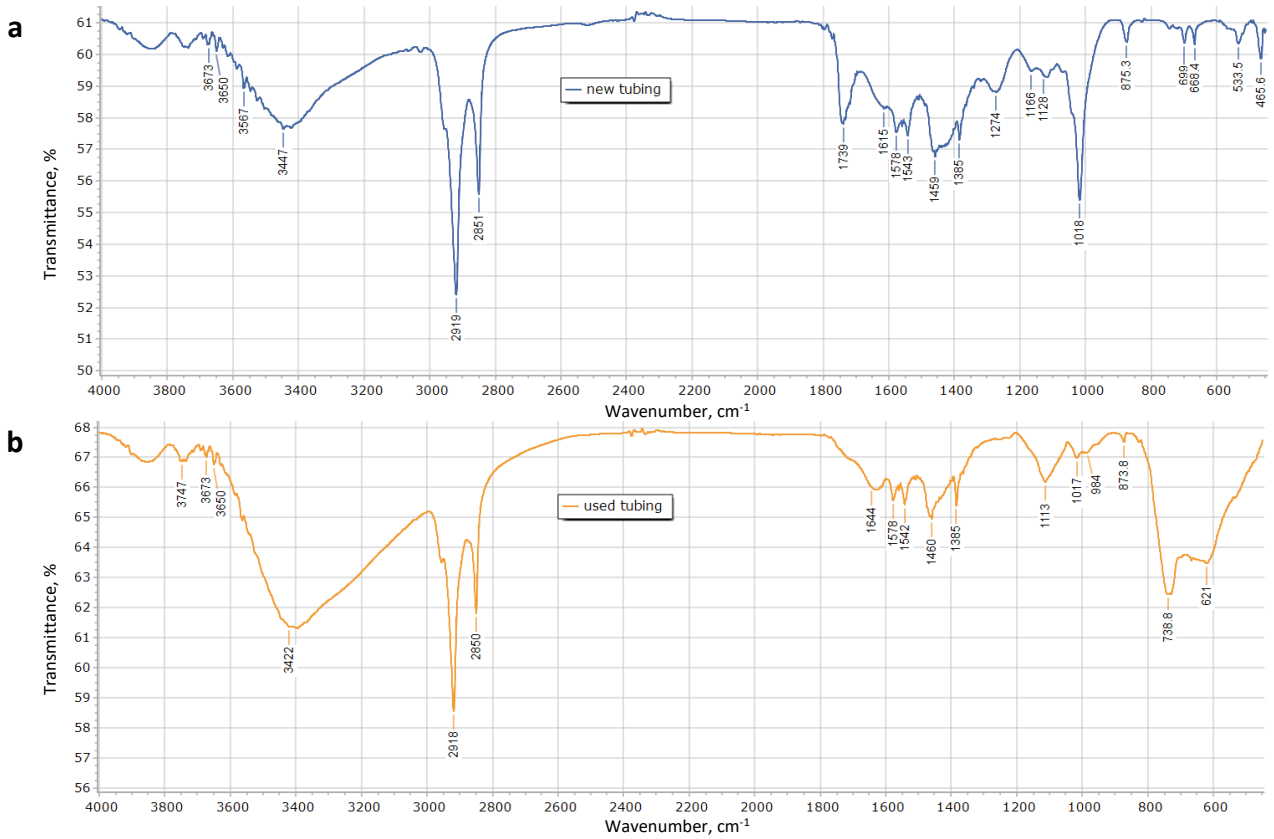

Figure 8. *FTIR spectra for a - new tubing and b - used tubing from the well*

Figure 9a shows a cracked but layer of antimony at the inner surface of the used CT (measurement point #1), located away from the analysed crack. The inner surface near the crack in

Figure 9b shows that no continuous antimony layer is present (measurement points #3 to #5), and in particular, no antimony is found within the pit (measurement point #2)

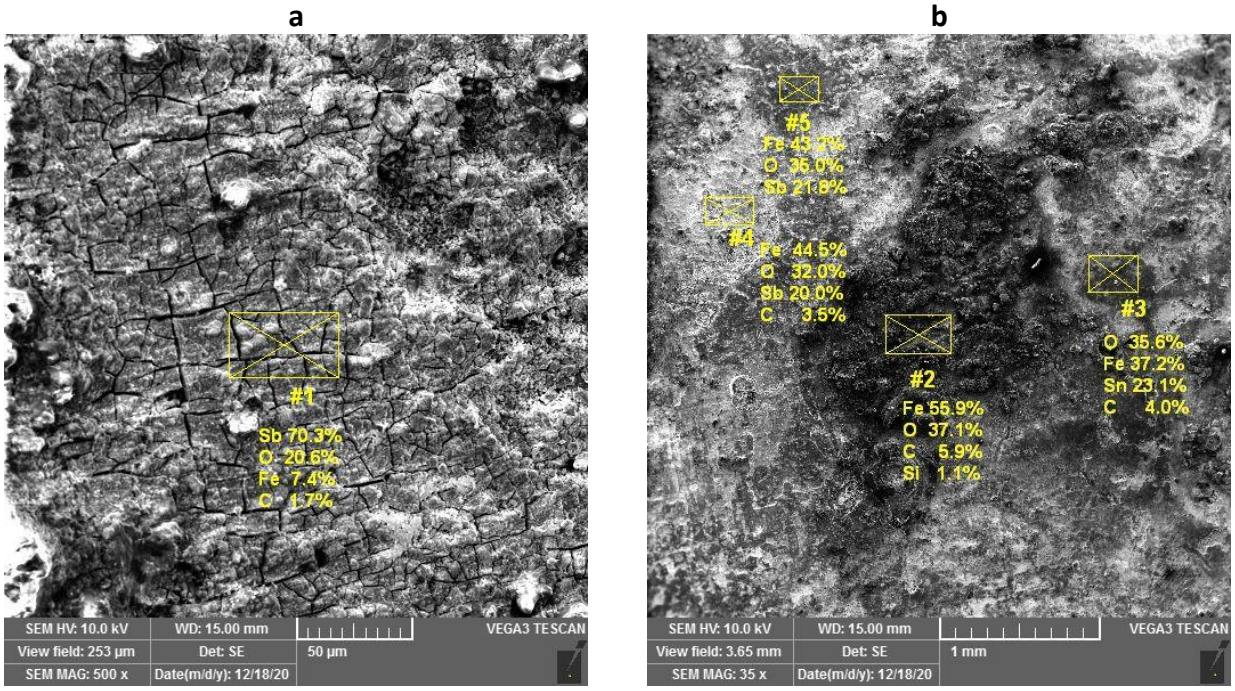

Figure 9. *Fine-grained structure of quasi-polygonal and needle ferrite with uniformly distributed areas of perlite and bainite*

The EDS was performed at different locations on the fracture surface (Figure 10). Representative EDS spectra are shown in Figure 11, and the results are summarized in Table 2. The EDS elemental analysis of the fracture indicates elements that can originate from the metal substrate (Fe, Cr, Si, C) or the environment (O, C, S, Si, Cl, Sb). Carbon can originate from the organic component of the corrosion inhibitor. Small amounts of sulfur were detected during the test. The sulfur could be from H_2S from the environment and/or microbiological corrosion induced by sulfate-reducing bacteria (SRB). However, the amount of sulfur is minimal and the source of the sulfur could not be clearly determined from this analysis. The presence of sulfides was not detected by the lead acetate paper test.

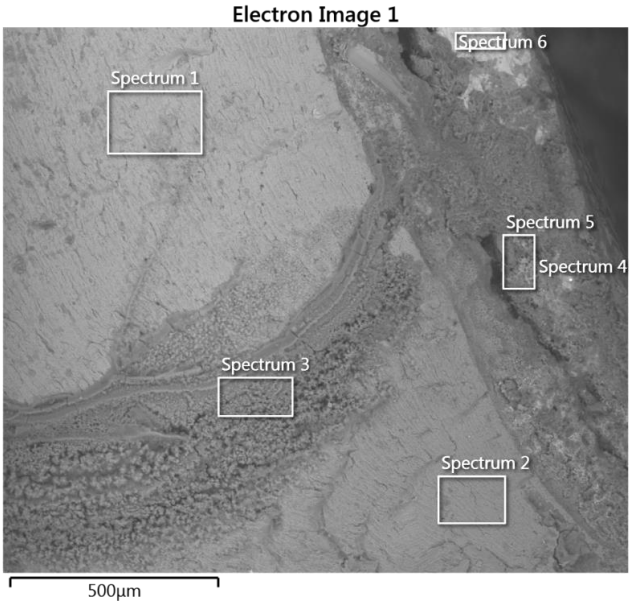

Figure 10. *EDS spectra locations at the fracture surface of the perforated sample*

Figure 12 shows the locations where the hardness measurements were made, and the results are summarized in Table 3. The hardness values were relatively consistent and agreed well with the declared value of 91.87 HRB (190 HV) of the CT-80 tubing parent material. Given the relatively small grain size (ASTM 13 to 14) and the fact that hardness decreases with decreasing grain size, this is the expected value of the measured hardness. H. Ghiasi [14] reported that the microstructure affects the improvement of properties and fatigue life. By decreasing the grain size, the mechanical properties and fatigue life increased.

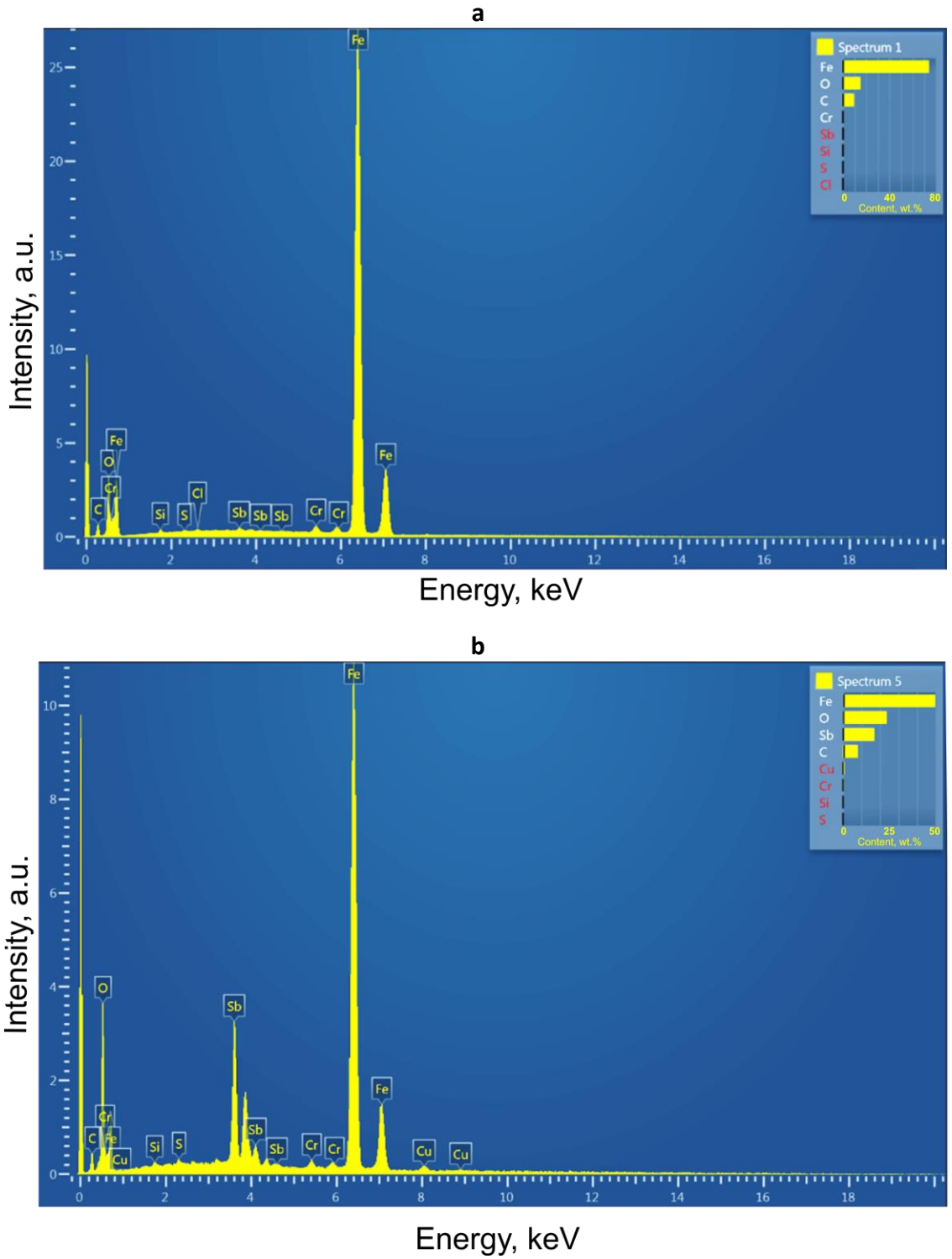

Figure 11. *Representative EDS spectra of the fracture surface in Figure 10 at different locations: a -location 1 and b - location 5*

Table 2. *EDS elemental analysis of the fracture surface at locations 1 through 6 in Figure 10*

Element	Content, wt.%					
	Fracture surface location					
	#1	#2	#3	#4	#5	#6
C	9.38	7.34	6.30	5.86	8.09	4.41
O	15.04	8.35	38.67	22.38	23.78	7.81
Si	0.32	0.62	0.42	-	0.22	-
Cr	0.58	0.67	-	-	0.52	-
Fe	74.04	83.03	54.26	11.61	50.14	3.24
S	0.10	-	-	-	0.18	-
Cl	0.09	-	-	-	-	-
Sb	0.44	-	0.34	60.14	17.06	84.53

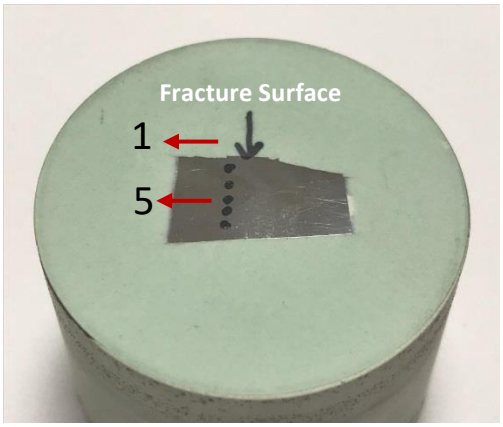

Figure 12. *Vickers microhardness examination sites*

Table 3. *Vickers hardness values near the fracture at different locations*

Location	HV	Location	HV
1	204	4	201
2	203	5	199
3	206	$\bar{x} \pm \sigma$	202.6 ± 2.7

Conclusions

- It can be concluded that pitting corrosion can occur on the inner surface of the tubing for two reasons:
  - during well acidizing, due to incomplete corrosion inhibition in 15% HCl,
  - during storage, between acidizing operations when the remaining liquid settles at the tubing bottom and causes pitting corrosion to occur.
- Given the appearance and location of the corrosion damage, the most likely cause of the fatigue cracks are corrosion pits that appear in the area of accumulation of residual electrolyte in the tubing during storage in atmospheric conditions.
- The pits at the inner wall serve as initiators of fatigue cracks and fractures that progress in the cycle of straightening and bending of the tubing.
- To prevent storage corrosion, it is necessary to properly maintain the tubing between acidizing operations by the following procedures:
  - nitrogen purging, preferably using a polyurethane ball to expel electrolytes from the tubing and subsequent capping the tubing ends,
  - application of vapor phase corrosion inhibitors.

References

[1] J. Abdo, A. Al-Shabibi, H. Al-Sharji, *Tribology International B* **82** (2015) 493-503. https://doi.org/10.1016/j.triboint.2014.01.028

[2] J. Li, J. Misselbrook, M. Sach, *Journal of Canadian Petroleum Technology* **49** (08) (2010) 69-82. https://doi.org/10.2118/113267-PA

[3] L. Garner, L. Vacik, S. Livescu, D. Blanco, *SPE/ICoTA Coiled Tubing and Well Intervention Conference and Exhibition*, Houston, Texas, USA, 2016 (SPE-179101-MS). https://doi.org/10.2118/179101-MS

[4] R. Hampson, E. Jantz, T. Seidler, *SPE/ICoTA Coiled Tubing and Well Intervention Conference and Exhibition*, Houston, Texas, USA, 2016 (SPE-179078-MS). https://doi.org/10.2118/179078-MS

[5] P. Brown, B. Gunby, C. Torres, *SPE/ICoTA Well Intervention Conference and Exhibition*, The Woodland, Texas, USA, 2019 (SPE-194306-MS). https://doi.org/10.2118/194306-MS

[6] S. Sherman, D. Brownlee, S. Kakadjian, *SPE/ICoTA Coiled Tubing and Well Intervention Conference and Exhibition*, The Woodland, Texas, USA, 2015 (SPE-173658-MS). https://doi.org/10.2118/173658-MS

[7] T. Padron and S. H. Craig, *SPE/ICoTA Coiled Tubing and Well Intervention Conference and Exhibition*, The Woodland, Texas, USA, 2018 (SPE-189914-MS). https://doi.org/10.2118/189914-MS

[8] W. D. Van Arnam, T. McCoy, J. Cassidy, R. Rosine, *SPE/ICoTA Coiled Tubing Roundtable*, Houston, Texas, USA, 2000 (SPE-60744-MS). https://doi.org/10.2118/60744-MS

[9] A. Syrotyuk, O. Vytyaz, R. Leshchak, J. Ziaja, *E3S Web of Conferences* **230** (2021) 01018. https://doi.org/10.1051/e3sconf/202123001018

[10] T. Padron, B. H. Luft, E. Kee, S. M. Tipton, *SPE/ICoTA Coiled Tubing and Well Intervention Conference and Exhibition*, The Woodland, Texas, USA, 2007 (SPE-107113MS). https://doi.org/10.2118/107113-MS

[11] D. Bronde, R. Edwards, A. Hayman, D.Hill, S. Mehta, T. Semerad, *Oilfield Review* **6(2)** (1994) 4-18. https://www.slb.com/-/media/files/oilfield-review/p04-18

[12] W. T. Becker, S. Lampman, *Fracture appearance and mechanisms of deformation and fracture*, in: *Volume 11, Failure Analysis and Prevention,* W. T. Becker, R. J. Shipley Eds., ASM International, 2002, 559-586. https://doi.org/10.31399/asm.hb.v11.a0003537

[13] J. W. Still, R. Rolovic, *A study of atmospheric corrosion of coiled tubing and Its Inhibition, Corrosion 2003,* San Diego, California, USA, 2003 (NACE-03593). ISBN: 03593 2003 CP

[14] H. Ghiasi, *Scientia Iranica* **25** (4) (2018) 2155-2161. https://dx.doi.org/10.24200/sci.2018.20677